

Optical and Morphological Study of Hydroxyapatite on Titanium Dioxide Particles for Photovoltaic Applications

Yunana Tanko¹, Haruna Ali² and Muhammad Y Onimisi²

¹ Department of Physics, Kaduna State college of Education Gidan Waya, Kaduna, Nigeria.

² Department of Physics, Nigerian Defence Academy, Kaduna, Nigeria.

Corresponding E-mail: yunanatanko01@gmail.com

Received 18-10-2022

Accepted for publication 20-10-2022

Published 11-11-2022

Abstract

In this study, a natural mineral termed hydroxyapatite (HA) ($\text{Ca}_{10}(\text{PO}_4)_6(\text{OH})_2$) was produced with TiO_2 stoichiometrically by normal sol-gel process. An investigation on how the different percentage weights of HA on TiO_2 can affect its optical and morphological properties were carried out, while the morphological nature and elemental composition was verified through scanning electron microscopy (SEM) and energy dispersive x-ray spectroscopy (EDX) analysis. Consequently UV-visible spectroscopy was used to measure the absorbance data, where optical constants such as absorption coefficient, extension coefficient, refractive index, transmittance, absorbance, thermal conductivity, the electron phonon interaction and steepness parameter were evaluated. According to the optical examination, the transmittance in the visible range is between (400 and 800 nm), and the absorption response in the UV region is between (200 and 400 nm) with an absorption edge occurring between (650 and 950 nm). The value of absorption coefficient (α) and extension coefficient (k) of HA/ TiO_2 increased with increase in the percentage weight (wt%) of HA. Equally, the optical conductivity increases with an increased in photon energy. In addition, the band gap energy decreases as the percentage weight of HA increases.

Keywords: Hydroxyapatite; titanium dioxide; optical band gap; steepness; nanoparticles; phonon.

I. INTRODUCTION

Nanocrystal line titanium dioxide (TiO_2) thin films have received a lot of attention in recent years due to their potential use as a low cost material in photovoltaics, gas sensors, photocatalysis, smart windows, antireflection coatings, optical filters, and dye-sensitized solar cells [7]. A variety of semiconductor photo catalysts, including TiO_2 , ZnS, Fe_2O_3 , CdS, GaP, and ZnO, have demonstrated their effectiveness by breaking down different organic pollutants in the presence of light by observing the band gap energy of the light [8]; among these, titanium dioxide (TiO_2) has gained an

interest in photocatalytic wastewater treatment owing to its thermal stability, and its higher chemical resistivity and robust mechanical properties [9-13]. Three crystalline forms of TiO_2 anatase (a), rutile (r), and brookite (b) as well as an amorphous form were discovered. These phases are easily recognizable considering their physical characteristics. The rutile and anatase phases are tetragonal in shape with the optical band gap of rutile (3.2 eV) less than that of anatase (3.0 eV). Anatase phase is known to exhibit better photocatalytic activity and is preferred over rutile for photodecomposition of environmental pollutants [14 -16], while the rutile phase exhibits better optical activity than anatase and is used for anti-

reflective and dielectric applications [17, 18]. However high dielectric constant of materials such as hydroxyapatite will enable the use of TiO₂ thin films in micro-electronic devices [19]. Amorphous, anatase, and rutile thin films' varied characteristics have sparked a lot of interest in the investigation of their growth methods and the measurement of their energy band gaps due to the remarkable variations in the optical characteristics of TiO₂ films caused by oxygen defects, impurities, and crystalline size. However, TiO₂ use was limited because of its poor adsorption of contaminants [20, 21] and significant recombination of photogenerated electron-hole pairs due to the band gap's proposed energy. [22, 23]. Furthermore, combining TiO₂ with substances like hydroxyapatite (HA), zeolite, silica, and activated carbon has been shown to improve the sample's optical and morphological characteristics, increase the active adsorption sites, and potentially speed up the mass transfer of mobility carriers and catalytic reactions. [24, 25]. However, hydroxyapatite (HA) Ca₁₀(PO₄)₆(OH)₂, is less expensive, has excellent mechanical stability, non-toxic and biocompatible [26]. It has hydroxyl ions (OH⁻) in its hexagonal structure, and in the presence of the necessary band gap energy, these OH⁻ ions may also boost electrical conductivity and charge carrier capacity. [27, 28]. Additionally, during the photocatalytic process, the PO₄ groups on the HA surface produce O₂ accept radicals, and these radicals may function as an electron receiver to achieve the separation of electron-hole pairs [29, 30].

Reference, [31] carried out an assessment of the structural, optical, and mechanical properties of the composite material for dental aesthetic application, as well as the effect of the nanostructured hydroxyapatite (NHAp) and titanium dioxide nanoparticles (NTiO₂) on dispersion in an adhesive containing monomers of dipentaerythritol penta-acrylate monophosphate (PENTA) and urethane dimethacrylate (UDMA). The mixture that resulted from the combination of NHAP 75%Wt – NTiO₂ %25Wt, at (10Wt%) into a dental glue, displayed the ideal aesthetic white appearance. They came to the conclusion that the nano composite PENTA/UDMA with nano hydroxyapatite and titanium dioxide combinations may be considered as a mechanical toughened, as well as a possible constituent that could be used to adjust shade attributes for dental aesthetic use but failed to give the details about the carrier mobility of the thin film at a different %wt of the nanocomposites of hydroxyapatite and titanium dioxide [31]. The manufacturing and characterization of hydroxyapatite/titanium nano composites for medical dental purposes have also been explored by [32]. TiO₂/HAp combination is promising in the field of biomedical applications as thin films which are mechanically separated. Furthermore, the use of TiO₂/HAp for enriching dental adhesives and photovoltaic application was discussed in [33]. Despite this stoichiometric analyses, further research is still required to fully comprehend the optical and morphological behavior of HA/TiO₂ in photovoltaic applications. Therefore,

it is anticipated that the creation of HA/TiO₂ composite will improve its optical characteristics, adsorption capacity, and reduce the recombination of the electron-hole pair created during the photocatalytic process. Therefore, the goal of this study is to evaluate the nature of the optical and morphological characteristics of HA/TiO₂ at various hydroxyapatite percentage weights. (0wt%, 30wt %, 40wt %, 50wt %, 60wt %, 70wt % and 80wt %), and its use in photovoltaic cells as a foundation for its development.

II. MATERIALS AND NUMERICAL METHOD

A. Materials

The materials used include 1.7244g per 20ml of TiO₂ solution, 4.311mg of HA per 2ml solution, glass slides of dimensions 2.5mm × 2.5mm all with 99.9% purity, and glass slide plate of 2.5mm × 2.5mm Titanium (IV) isopropoxide [C₁₂H₂₈O₄Ti] (TTIP). Serum plain micro point diagnostics vacuum tube. Propanol, acetic acid and orthophosphoric acid [H₃PO₄]. Calcium to phosphate ratio (ca/pa) 1.65 – 67.

B. Method

1) Preparation of HA/TiO₂ Composite Thin Film and Characterization

The source material for titanium (Ti) was titanium (IV) isopropoxide [C₁₂H₂₈O₄Ti] (TTIP), which had a purity level of 99.99%. The solvents utilized were propanol and double-distilled water (dH₂O), while the stabilizing agent used was acetic acid. Solaronic provided the propanol, acetic acid, and orthophosphoric acid [H₃PO₄]. Tiny glass slides with dimensions of 2.5 mm × 2.5 mm were employed as substrates. The substrates were first cleaned with soap solution for 5 min, and then they were placed in a hot bath of chromic acid for 20 min at 50°C. The substrates were then rinsed with distilled water and cleaned with an ultrasonic cleaner. The stoichiometric analysis of 1.7244 g per 20 ml of TiO₂ solution, which included 2930 g, was combined with a proportion of 4.311mg of HA per 2 ml of solution to produce a prepared solution of HA/TiO₂ nano composite. By stoichiometric analysis, the weight percentages of HA (0, 30, 40, 50, 60, 70, and 80) with an equivalent volume of TiO₂, were obtained while (1) was used to determine the appropriate mass of HA in grams.

$$wt\% = \frac{x}{(4.311+x)} \quad (1)$$

Similarly, (2) was used to obtain the volume of TiO₂,

$$V_{TiO_2} = 20 \times \frac{x}{2930} \quad (2)$$

Where x stands for equivalent mass (m/g) of HA and TiO₂.

Drops of 20 ml TiO₂ and propanol suspension were added to the HA mixture at various percentages, and the mixture was rapidly agitated for 2 hrs. The reaction mixture was ultrasonically treated using 60W Bath Sonicator, PCI

Analytics, for a further 4 hrs. The reaction mixture was then centrifuged at 6000 RPM for 20 mins to collect the produced HA/TiO₂ composites, and then autoclaved for 8 hrs at 190°C. The TiO₂ film was deposited on the slide glass to fabricate a 4 nm thick film; thereafter HA was coated to obtain a 4 nm thickness. The total film thickness was 8 nm. In addition, the film was annealed in air for four hrs at 350 °C in an electric furnace. Using XRD (RINT2000, Rigaku Corp., Japan), the crystallinity of the films was assessed using a Cu K radiation source operating at 45 kV and 40 mA excitation current. Furthermore, a Thermo scientific Evaluation 300 UV- Vis absorption spectrophotometer (300UV; Jasco Corp., Japan) was used for the optical characterization. The thin films obtained at different percentage weight of HA is shown in Table I.

Table I Thin films obtained at different percentage weight of HA

Sample code	HA/TiO ₂ Compositions			Sample Image
	HA wt%	HA (m/g)	TiO ₂ (ml)	
HA/TiO ₂ 1	0	0	0	
HA/TiO ₂ 2	30	1.847	20	
HA/TiO ₂ 3	40	2.874	20	
HA/TiO ₂ 4	50	4.311	20	
HA/TiO ₂ 5	60	6.466	20	
HA/TiO ₂ 6	70	10.059	20	
HA/TiO ₂ 7	80	17.244	20	

2) Theories for HA/TiO₂ Evaluation

Absorbance (A) is the ratio of the amount of light absorbed by the sample (IA) to the amount of light incident on it (IO).

$$A = \frac{IA}{IO} \tag{3}$$

Transmittance T is given by

$$T = e^{(-2.303A)} \tag{4}$$

Reflectance R is calculated as in (5)

$$R = 1 - (A + T) \tag{5}$$

The reflectance data is used to calculate the refractive index (η) of the thin film using (7)

$$R = \frac{(\eta-1)^2}{(\eta+1)^2} \tag{6}$$

$$\eta = \frac{(1+\sqrt{R})}{(1-\sqrt{R})} \tag{7}$$

The extension coefficient (k) was calculated using (8).

$$\bar{\eta} = \eta + ik \tag{8}$$

Where η is the real refractive index, $\bar{\eta}$ is the complex refractive index and k is the imaginary part named as extinction coefficient. Extinction coefficient provides information about the absorption of light in material medium

due to inelastic scattering. It is known that extinction coefficient and absorption coefficient can be related by (9).

$$k(\lambda) = \frac{\alpha(\lambda)\lambda}{4\pi} \tag{9}$$

Where, $k(\lambda)$ is the extinction coefficient, $\alpha(\lambda)$ is the absorption coefficient and λ is the wavelength.

The complex permittivity is divided into two parts: real dielectric constant (ϵ_1) and imaginary dielectric constant (ϵ_2) given by (10)

$$(\epsilon_x) = (\epsilon_1) + i(\epsilon_2) \tag{10}$$

The real and imaginary parts of the complex permittivity are related to (η) and (k) as given (11) and (11).

$$\epsilon_1 = \eta^2 - k^2 \tag{11}$$

$$\epsilon_2 = 2\eta k \tag{12}$$

The optical conductivity is calculated using (13)

$$\sigma_{opt} = \frac{\alpha nc}{4\pi} \tag{13}$$

Where α is the absorption coefficient, η is the refractive index and c is the velocity of light.

Band gap is generally determined using the absorption coefficient in Tauc method. In this method, the absorption coefficient and thickness of the layers are generally required to determine the band gap. The Tauc equation for measuring band gap energy was used in this study and is given by (14) [34-35].

$$\alpha(h\nu) = A(h\nu - E_g)^n \tag{14}$$

In optical absorption, an electron from the top of the valence band is typically stimulated into the bottom of the conduction band across the energy band gap, close to the band boundaries. If these electrons experience disorder during this transition process, it results in density of their states given as $\rho(h\nu)$, where $h\nu$ is the photon energy tumbling into the energy gap and ρ is the electron density of state. This tail of $\rho(h\nu)$ extending into the energy band gap is termed as Urbach tail. Consequently, absorption coefficient $\alpha(h\nu)$ also tails off in an exponential manner and the energy associated with this tail is referred to as Urbach energy and can be calculated using (15).

$$\alpha(h\nu) = \alpha_o e^{hv/E_u} \tag{15}$$

Where α_o is a constant, $h\nu$ is the photon energy and E_u is the Urbach energy.

III. RESULTS AND DISCUSSION

Fig. 1, depicts the optical absorption spectra of HA/TiO₂ composite thin films with percentage weights (wt %) of 0, 30, 40, 50, 60, 70, and 80 based on the absorbance information

from the UV-visible spectrometer, which was recorded in the spectrum of wavelengths spanning from 400 nm to 1100 nm.

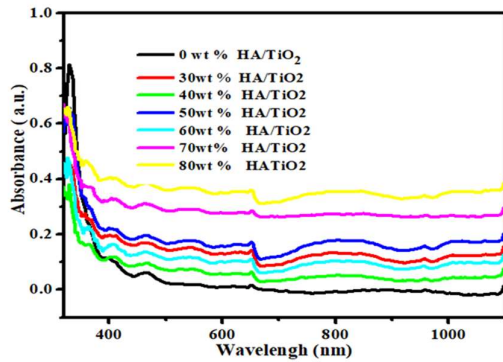


Fig. 1 optical absorbance of HA/TiO₂ at different wt %.

The strong reaction in the UV area was seen to occur between 200 and 400 nm, with the absorption edge occurring between 650 and 950 nm. The reason for the absorption edges of HA/TiO₂ at 650 nm is due to the charge transfer from the valence band to the conduction band of the Ti⁴⁺ cations, as a result of enhancement of HA/TiO₂ films compactness (shrinkage of the bond length). This is in agreement with research done by [36]. In addition, the broad intense absorption edge of the spectrum is as a result of formation of anatase nanoparticles. Here, the absorption band corresponding to the HA/TiO₂ nano composites gets blue shifted, the shift of the absorption band towards shorter wavelength indicates decrease in particle size, while the absorption edges get red shifted indicating an increase in the particles size of HA that are active in TiO₂ layer, which is also consistent with the result of [36]. Equation (5) was used to calculate the optical transmittance of HA/TiO₂ at various weight percentages. The presence of 0 weight percent of HA particles on TiO₂ was observed to have a maximum transmittance of greater than 95% in the visible light band (400 - 800 nm). Low HA particle density results in small particle sizes, which opens up more possibilities for high transmittance capacitance at 0 weight percent of HA/TiO₂ layer. Contrarily, spectra transmittance sharply decreased at the UV region, leading to an obvious absorption edge being observed at 680 nm. This could be due to an increase in the percentage weight of HA on TiO₂, which results in larger particle size that will trap the UV- light and reduce the degree of transmittance in HA/TiO₂ and is consistent with the results of [37]. After subsequent percentage weight of HA on TiO₂ and moderate heat treatment, the transmittance of the HA/TiO₂ film decreased by around 8% in the visible light region. This is because the crystal grain grows with heat energy. In addition, it was reported by [37] that the grain size of TiO₂ film increase with annealing temperature from an atomic force microscopy observation, and the transmittance of

the film decreased. Fig. 2 demonstrates that the HA/TiO₂ film has an average transmittance of 97% in the visible spectrum, which is still a high transparency.

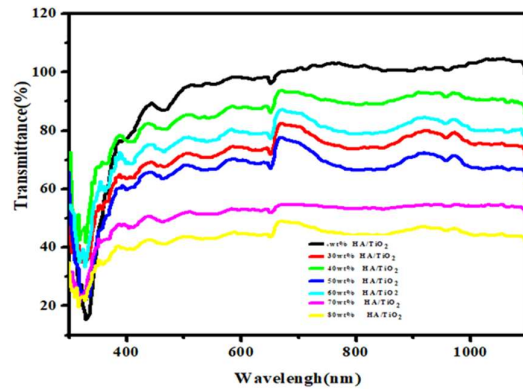


Fig. 2 Optical transmittance of HA/TiO₂ at different wt %.

A. Optical Constant of HA/TiO₂

Equation (9) was used to calculate the variation in absorption coefficient with wavelength for various weight percentages of HA at wavelengths between 300 nm and 1200 nm. Different weight percentages of HA/TiO₂ were absorbed at the same wavelength and with identical absorption edge values in the ultraviolet region of the electromagnetic spectrum. Fig. 3 shows that the absorption increases as the weight percentage of hydroxyapatite increases in TiO₂, except at 0% and 40%, where there is an abnormality with a higher absorption coefficient value (36000000 and 25000000). This may be due to a lack of or a small percentage of hydroxyapatite nanoparticles, which could disperse uniformly in the matrix with enough TiO₂ proportion and significantly lessen the agglomeration effect of the hydroxyapatite nanoparticles. Thus increasing the absorption coefficient with little or no HA nanoparticles, which is consistent with findings of [38].

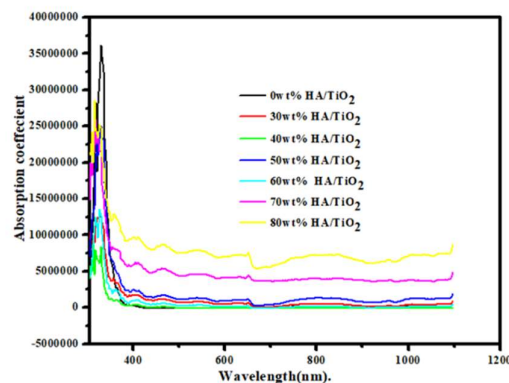


Fig. 3 Variation of Absorption Coefficient of HA/TiO₂ with Wavelength at different wt % of HA.

Furthermore, an increase in the size of the active particles may boost the charge transfer of the Ti^{4+} cations from their valence band to their conduction band, resulting in an increase in the absorption capacity of HA/TiO₂. This was in line with the outcome of [35]. The extension coefficient (k) of HA/TiO₂ is shown in Fig. 4 at various weight percentages of HA. It is defined as the portion of energy lost by scattering and absorption per unit thickness in a specific medium of HA/TiO₂, and it was calculated by means of (10) using the absorbance data. It is evident that the extension coefficient is large at 0 weight percent and low at 40 weight percent of HA. Fig. 4 depicts the relationship between the absorption coefficient (k) of HA/TiO₂ and wavelength. These values were observed to rise when HA weight percentage increased (up to 80 wt%). According to [37], the tiny weight percentage of HA shows that the composite samples are still transparent to electromagnetic radiation, which increases the extension coefficient. However, it is clear that there is some interaction between photons and the films electrons from the variation in the refractive index (η) and extension (k) values with wavelength for HA/TiO₂. Additionally, an increase in extension coefficient (k) values at high wavelength for wt% of HA suggests that more photons are scattered when HA is introduced, which is consistent with the findings of [38].

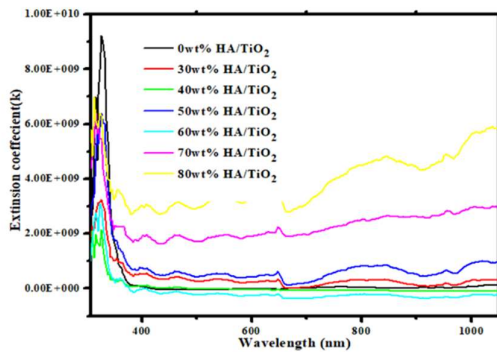


Fig. 4 Variation of Extension coefficient (k) of HA/TiO₂ with wavelength at different wt % of HA.

Fig. 3 and 4 show the values of HA/TiO₂ absorption coefficient (k) and extension coefficient (k) at a specific wavelength of 300 nm. These numbers indicate a rising trend in the weight percentage of HA. This is consistent with the work of [37, 39]. Fig. 5 shows the refractive index dispersion (η) for several doped HA/TiO₂ materials at wavelengths between 300 and 1100 nm, which were calculated from the absorbance values using (8). The refractive index (η) rises with increasing % wt of HA thin films up to 0.325 in HA/TiO₂, and the increase in thin film dispersion occurs at 0% of HA/TiO₂ (see Fig. 5). Additionally, it has a high wavelength value with its lowest refractive index at 40 wt % HA and greatest refractive index at 0 wt% HA, respectively.

According to [40], the refractive index (η) is tunable upon addition of several wt% of HA on a substrate as evidenced by the increase and reduction in refractive index (η) with increasing wt% of HA/TiO₂. As can be seen from Fig. 5, the refractive index drops sharply as wavelength rises and becomes saturated above a wavelength of 1000 nm. The bulk qualities of the material are represented by the high wavelength area of the refractive index (η). The percolation threshold phenomena may be responsible for the abrupt rise in refractive index (η) for TiO₂ volume and weight percentage of HA; this is in line with [41].

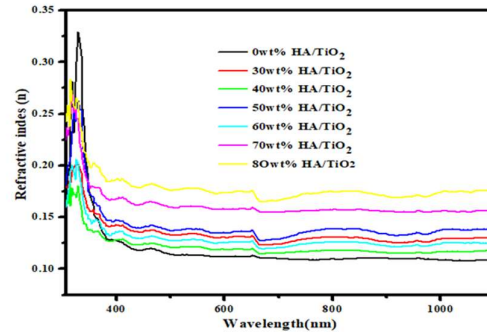


Fig. 5 Variation of Refractive index (η) with Photon Energy of HA/TiO₂ at different wt % of HA

B. Optical Conductivity.

Fig. 6 shows how the optical conductivity (opt) of thin films made of HA/TiO₂ varies with photon energy. The optical conductivity of HA/TiO₂ thin films at several wt % of HA is clearly shown to rise with an increase in photon energy. Since the optical conductivity (opt) was calculated using the absorption coefficient, an increase in the optical conductivity at high photon energies may be caused by the high absorbance of HA/TiO₂ thin films as well as by electrons that are excited by the energy of the photons due to an increase in the weight percentage of HA, which in turn increases the number of mobility carriers and thus the conductivity. This is consistent with [42].

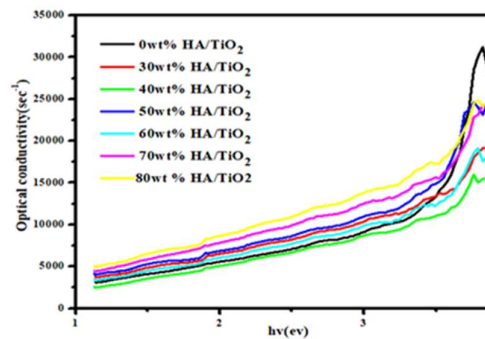


Fig. 6 Variation of Optical Conductivity (sec^{-1}) with Photon energy of HA/TiO₂ at different wt% of HA.

Optical conductivity is at a minimum level of $(25000-5000) \text{ sec}^{-1}$; this low value is a result of a reduction in charge carrier mobility due to ionic size, which, in turn, causes a change in the electronic band structure. As electrical conductivity is proportional to carrier concentrations and mobility, the optical conductivity of HA/TiO₂ thin films is seen to increase with increase in applied energy. This is consistent with the study carried out by [43].

C. Optical Band Gap Energy

Fig. 7 display the Tauc method for band gap determination of HA/TiO₂ at different percentage weight of hydroxyapatite (wt%).

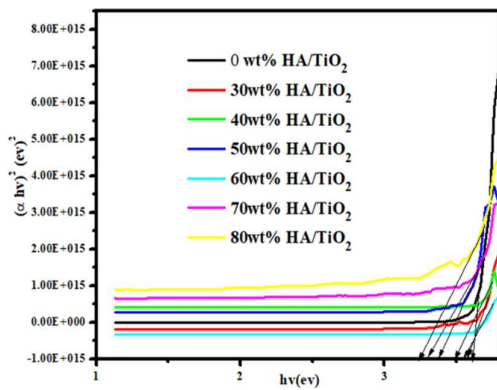


Fig. 7 Variation of $(ahv)^2 (eV)^2$ against $hv (eV)$ optical bandgap of HA/TiO₂ at different HA wt%.

The band gap energy is obtained by extrapolating the linear portion of a curve and intersecting it with the horizontal axis, there by estimating an appropriate value for each percentage weight of HA using (14), and the value of estimated band gap energy is shown in Table II.

Table II. Optical bandgap, Urbach energy, steepness parameter and electron phonon interaction parameter values.

S/N	HA	$E_g (eV)$	$E_u (eV)$	σ	E_{e-p}
1	0	3.61	15.22	9.071×10^{-25}	6.047×10^{-25}
2	30	3.57	1.10	3.765×10^{-22}	2.51×10^{-23}
3	40	3.51	3.97	1.39112×10^{-22}	9.27×10^{-23}
4	50	3.38	4.28	1.6129×10^{-22}	1.07526×10^{-22}
5	60	3.58	1.74	4.761×10^{-22}	2.853×10^{-22}
6	70	3.25	7.07	1.367×10^{-22}	9.11×10^{-23}
7	80	3.22	8.54	1.2933×10^{-22}	8.62×10^{-23}

The analysis proved that, at 0 wt% and 30 wt% HA/TiO₂ the band gap energy has an estimated value of 3.61 eV and 3.57 eV. In addition, at 40 wt%, 50 wt% and 60 wt% the observed value of band gap energy at each point is 3.51 eV, 3.38 eV, and 3.56 eV respectively. However, as the percentage weight of HA/TiO₂ increases to 70 and 80 the estimated value of band gap was observed to be 3.23 eV and 3.25 eV. From results obtained, it's clearly shown that,

the band gap of a materials decreases as the percentage weight of hydroxyapatite increases within a range of (3.61 – 3.25) eV, except at 60wt% with an increase in the band gap value of about 3.56 eV. The lower value of E_g is attributed to the creation of allowed energy states in the band gap [45, 46] as a result of increase in particles size at the time of film preparation, while the higher value of E_g is accounted to the very small grain size of the film leading to an increase in the grain boundary, hence increase in the band gap energy. This is in agreement with the research conducted by [46, 47].

Fig. 8 is the plots of $\ln(\alpha)$ versus photon energy, showing the distortion that occurs at different percentage weights of hydroxyapatite on titanium dioxide. Its values were achieved by determining the reciprocal of the slope from the linear region of the graph. Three different types of absorptions are used to categorize the significant elements of Fig. 8 (a, b, c, d, e, f, and g). The first is the WAT (Weak Absorption Tail) area, which is attributed to the modest optical absorption (α) controlled by optical transitions from one tail state to another tail state.

The second is Region-U, which agrees with [47] and is where transitions from localized tail states above the valence band to extended levels in the conduction band and/or from extended states in the valence band to localized tail states below the conduction band control. The spectral dependency of this area adheres to the Urbach rule. The third is Region-T, which shows the range of controlled by optical transitions between one extended state and another extended state, which occur at various percentage weights of HA/TiO₂. The majority of the semiconductors in this region that are amorphous and nanocrystal line follow Tauc's relation. As a result, the level of increase in WAT and Urbach energy can be utilized to quantify the degree of disorder in the films. From Fig. 8 (a), the obtained Urbach energy value was calculated to be 15.22 eV at a percentage weight of 0 % HA. However, as the percentage weight of HA increased to 30 wt% , 40 wt% and 50 wt% , as shown in Fig. 8 (b, c, and d), there was a consistent increase in the Urbach energy, with Urbach values of 1.10 eV, 3.97 eV, and 4.28 eV, respectively. The Urbach energy value was then estimated to be 1.74 eV, 7.07 eV, and 8.84 eV, respectively, as the weight percentages of HA were increased to 60 wt%, 70 wt%, and 80 wt% as shown in Fig. 8 (e, f, and g). The increase in Urbach energy was often seen to occur in two stages, the first of which is depicted in Fig. 8 (b, c, and d) at 30 wt%, 40 wt% and 50 wt% at a specified range of Urbach values of (1.10 – 4.28) eV. While the second stage occur at (60, 70, and 80) wt% HA at an estimated Urbach value ranging from (1.74 to 8.84) eV as depicted in Fig. 8 (e, f, and g). The degree of disorderliness of thin films is clearly shown to increase at each stage as the weight percentage of HA increases, with the exception of the zero weight percentage, which exhibits a high degree of disparity that may be caused by a higher density of the localized state, according to [48].

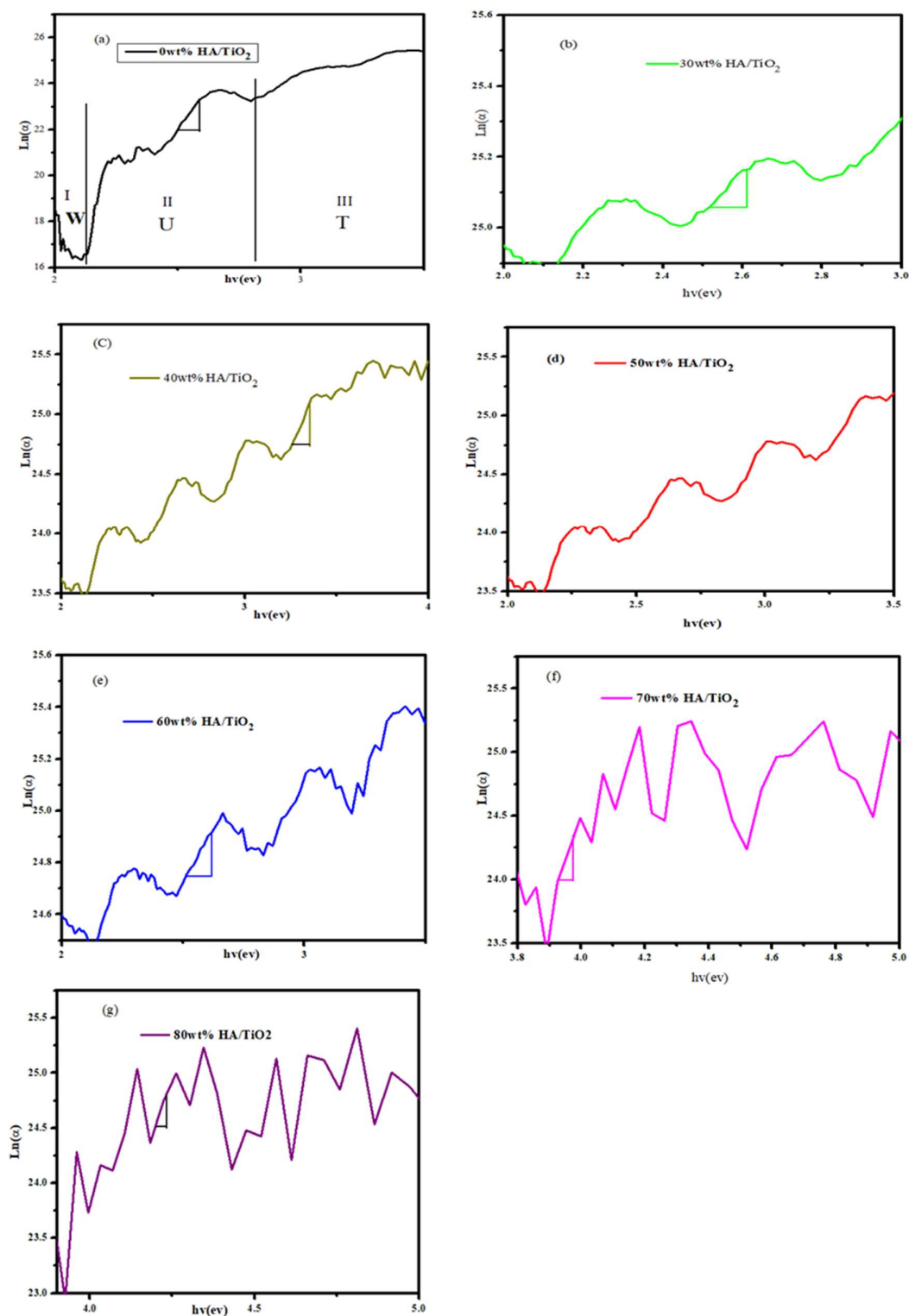


Fig. 8 plot of $\ln(\alpha)$ versus $h\nu$ (eV). Urbach energy of HA/TiO₂ at different HA wt% (a) 0 wt% (b) 30 wt% (c) 40 wt% (d) 50 wt% (e) 60 wt% (f) 70 wt% (g) 80 wt%.

The degree of disorderliness of thin films is clearly shown to increase at each stage as the weight percentage of HA increases, with the exception of the zero weight percentage, which exhibits a high degree of disparity that may be caused by a higher density of the localized state, according to [48]. In accordance with [49], it can also be assumed that increases in the Urbach energy are the result of more defects or table dangling bonds between HA and TiO₂. The increased disorderliness may be caused by an increase in grain size, which causes a crystal to dislocate, increasing the disorder of the thin film. This was in line with the outcome of [50].

The relation between the bandgap energy and the width of Urbach tail is shown in Fig. 9 for films deposited at HA = 0 wt%, 30 wt%, 40 wt%, 50 wt%, 60 wt%, 70 wt% and 80 wt%. The bandgap reduces as E_u grows, with the exception of 30 and 60 wt%, where there is a tiny value of Urbach energy, which may be due to the thin film's reduced disorderliness. Therefore, a linear fit was created. The

decrease in band gap as the Urbach energy increases may be caused by an increase in the dispersion of grain size. This drop in bandgap results in an infinitesimal band tailing. The bandgap energy at $E_g = 0$ or the bandgap in the absence of tailing is represented by the constant A resulting from the fit. The obtained values are 3.64664 eV for the substrate at different percentage weight of HA and this values correspond with the value of band gap energy at the initial stage. So the bandgap value in the case of no tailing decreases with the increase in the substrate percentage weight of HA, which is in accordance with the known situation of semiconductors. This result supports our aforementioned explanation on the decrease of bandgap energy with an increase in percentage weight of the substrate. In other words, films with a higher percentage weight of HA have more order and a lower density of localized states. The slope of the straight lines is equal to -3.899 . This linear relationship between bandgap energy and Urbach tail diameter was also discovered by [51].

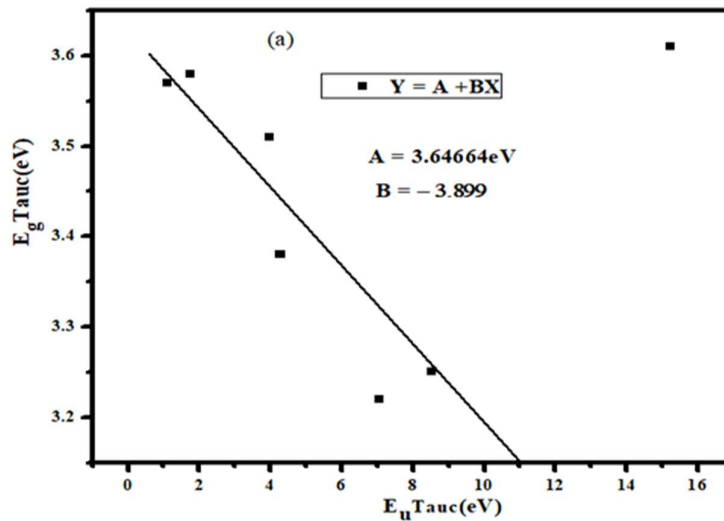


Fig. 9 relation between the bandgap energy and the width of Urbach tail for HA/TiO₂ thin films deposited at different percentage weight.

D. Morphological Characterization.

For the investigation of the morphological characteristics of the thin films that were deposited at various wt% HA, scanning electron microscopy (SEM) was used, as shown in Fig. 10. It is clear that spherically-shaped nano scale HA/TiO₂ particles with various HA content weights have fully covered the glass substrate. Because the crystallites generated from the solution at low deposition rates had well-defined multi-grain agglomerates with unequal shape and size, it was found that the influence of low %wt deposition of HA on TiO₂ a tiny crystal size could be plainly seen demonstrating a tiny area of nano particle aggregation. A consistent semi-spherical TiO₂ and HA particle structure was also observed to evolve as the

size of the nanoparticles in the films increased due to an increase in the weight percentage of HA. This clearly shows how TiO₂ was impacted by various HA %wt. The fact that the growth of TiO₂ microspheres was initially reduced by the hydroxyapatite nanoparticles by prematurely stopping the growth process, as illustrated in Fig. 10 in 0 wt% and 30 %wt HA.

Also, irregularly shaped particles were changed to semi-spherical particles as percentage weight of HA increased. However, despite the rather thick HA/TiO₂ coatings becoming more durable as the HA percentage weight grew, numerous cracks still showed up on them. In general, small titanium

grain aggregates caused the formation of nucleation centers that ranged in weight percentage from 0 %wt to 40 %wt, but more significantly, complete covering of the underlying HA/TiO₂ was seen when the percentage weight reached 50 %wt, uniform dispersion at the surface of titanium particles was then seen, which is consistent with [52]. The fact that as the percentage weight of HA increases from

(60 to 80 %wt), the film thickness increases along with an increase in particle size, where the TiO₂ particle dominates the HA particle in thin films due to uniform distribution of HA nanoparticle on TiO₂ which may lead to a better association for electron phonon interaction, thereafter given a better foundation for a photovoltaic cell.

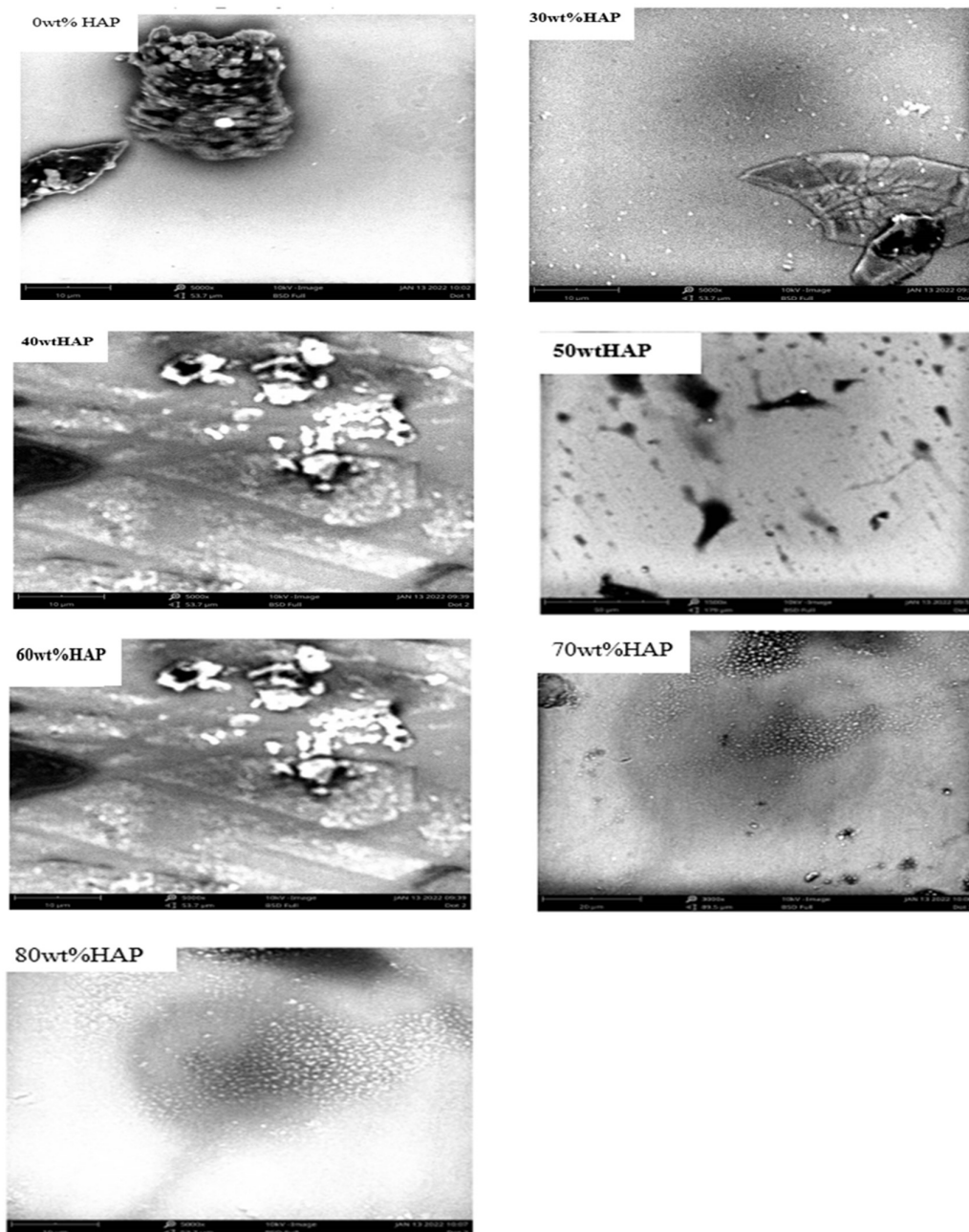


Fig. 10 SEM images of HA/TiO₂ composite thin films at different %wt of HA

E. EDX Analysis

An energy dispersive x-ray spectroscopy (EDX) analysis is recorded during the SEM analysis which gives information about the elemental composition. The EDX spectrum was captured with a working distance of 12.9 mm and an accelerating voltage of 15 keV. The EDX spectrum was acquired from the top view of a nano composite film made up of 60 %wt HA/TiO₂ as depicted in Fig. 10 with the aid of a fast moving electron X-ray signals. When compared to the peaks that belong to P, which are gathered at 2.0 keV, the oxygen peak at 0.5 keV shows that Oxygen is the dominant peak with a percentage weight concentration of roughly 6.5 keV compared to the peaks corresponds to P which is collected at 2.0 keV. The absence of the calcium and Ti peaks is due to the host and dopant's high absorption capacity, which occurs at a clearly steep point at 60 %wt of HA, as shown in Fig. 11. P, C, Si, Na, and O are present in the top portion of the HA/TiO₂ nano composite film layer of the sample. The EDX analysis clearly revealed the presence of main elements of the composites is P, and O. and nonappearance of Ca and Ti due to the high degree of steepness value at 60 wt% of HA.

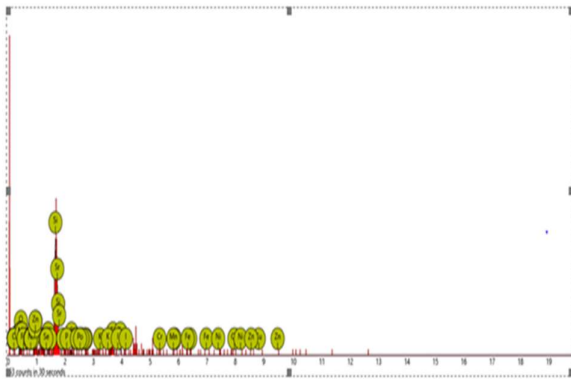


Fig. 11 EDX profile of HA/TiO₂ composite thin film of HA

F. Estimation of Steepness Parameter and Strength of Electron-Phonon Interaction

To ascertain the deep information about defect density and relaxation of distorted bonds, these were fully achieved by evaluating steepness parameter and strength of electron-phonon interaction. The supporting information includes information on the steepness parameter, the strength of the electron-phonon interaction, and the relevance of each. The following equations are used to estimate the steepness parameter (σ) and the strength of the electron-phonon interaction (E_{e-p}).

$$\sigma = \frac{K_B HAP}{E_u} \tag{16}$$

$$E_{e-p} = \frac{2}{3\sigma} \tag{17}$$

The calculated values of σ and E_{e-p} are listed in Table II. The changes in steepness parameter and strength of electron-phonon interaction with increase in percentage weight of hydroxyapatite is shown in Fig.12. The plot demonstrates that the strength of the electron-phonon interaction decreased as the steepness of the thin films parameter rose with the elevation of %wt HA. This could be due to an improvement in crystallinity in the film, which is indicated by an increase in the percentage weight of hydroxyapatite. This change is also connected to decrease in defect density states close to the exponential absorption edge and the relaxation of deformed bonds [53].

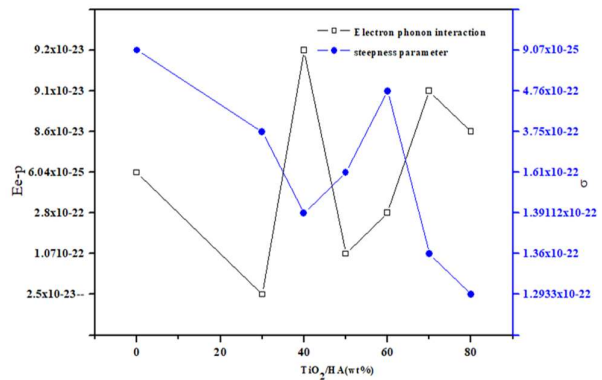


Fig. 12 Variation of σ and E_{e-p} of HA/TiO₂ films with different wt% Hydroxyapatite.

IV. CONCLUSION

The optical and morphological properties of hydroxyapatite on titanium dioxide particles for photovoltaic applications was examined. HA/TiO₂ thin films with various HA concentrations were synthesized and examined, with results indicating that as the percentage weight of HA grows, optical parameters including transmittance, absorbance, absorption coefficient, extension coefficient, and refractive index increase respectively. Additionally, the band gap energy values drop as the percentage weight increases, whereas the thermal conductivity increases with an increase in photon energy. The observed maximum band gap energy was 3.61 eV, while the Urbach energy was between 15.22 and 8.54 eV, increasing at a rate of 30 % to 50 %, then declining at 60%, and then increasing at a rate of 70% to 80%. The relationship between the bandgap energy and the width of the Urbach tail was examined, and it was found that as the value of E_u increases, the bandgap decreases with the exception of at 30 wt% and 60 wt%, where a small value of Urbach energy is present. This low value of Urbach energy may be due to the thin film's reduced

disorderliness. The obtained values are 3.64664 eV for the substrate at various percentage weights of HA. Additionally, semi-spherical TiO₂ and HA particles were discovered with increasing film nanoparticle sizes, according to morphological investigations. Additionally, it was thoroughly demonstrated that the strength of the electron-phonon interaction and the steepness parameter both changed when the percentage weight of hydroxyapatite rose. This is because the percentage weight of HA increased together with the steepness of the thin films parameter and the electron-phonon interaction become weaker.

ACKNOWLEDGMENT

The authors wish to express their gratitude to staff of the Nigerian Defense Academy Kaduna, for their support during the laboratory investigations. We also appreciate Kaduna state government's financial support for the project.

References

- [1] V. Maurice, T. Georgelin, J. M. Siaugue, V. Cabuil, "Synthesis and characterization of functionalized core-shell gamma Fe₂O₃-SiO₂ nanoparticles". *J. of Magnetism and Magnetic Mat.*, vol. 321, no. 10, pp. 1408–1413, 2009.
- [2] H. Bala Y. Zhang, H. Yang, C. Wang, M. Li, X. Lv, and Z. Wang, "Preparation and characteristics of calcium carbonate/silica nanoparticles with core-shell structure". *Colloids and Surfaces A: Physicochemical and Engineering Aspects*, vol. 294, no. 1, pp. 8-13, 2007.
- [3] M. Okada, Y. Yamada, P. Jin, M. Tazawa and K. Yoshimura, "Fabrication of multifunctional coating which combines low-e property and visible-light-responsive photocatalytic activity". *Thin Solid Films*, vol. 442, no. 1, pp. 217-221, 2003.
- [4] A. Ennaoui R. Sankapal, V. Skryshevsky and M. C. Lux-Steiner, "TiO₂ and TiO₂-SiO₂ thin films and powders by one-step soft-solution method: Synthesis and characterizations". *Solar Energy Mat. & Solar Cells*, vol. 90, no. 10, pp. 1533-1541, 2006.
- [5] R. Weinberger and B. Garber, "Titanium-dioxide photocatalysts produced by reactive magnetron sputtering". *App. Phys. Lett.*, vol. 66, no. 18, pp. 2409-2411, 1995.
- [6] D. Manno, G. Micocci, R. Rella, A. Serra, A. Taurino and A. Tepore, "Titanium oxide thin films for NH₃ monitoring: Structural and physical characterizations". *J. of App. Phys.*, vol. 82, no. 1, pp. 54-59, 1997.
- [7] A. Ramadoss and S. Kim, "Vertically aligned TiO₂ nanorod arrays for electrochemical super capacitor". *J. of Alloys Comp.*, vol. 56, no. 1, pp. 262-267, 2013.
- [8] J. Seo Jeong and C. Lee, "Photocatalytic degradation of organic compounds by 2-ethylimidazole-treated titania under visible light illumination". *Membr. Water Treat.*, vol.10, no.3, pp. 9–223, 2019.
- [9] S. Mozia, P. Sienkiewicz, K. Szymański, M. Zgrzebnicki, D. Darowna, A. Czyżewski and A. W. Morawski, "Influence of Ag/titanate nanotubes on physicochemical, antifouling and antimicrobial properties of mixed-matrix polyethersulfone ultrafiltration membranes". *J. of Chem. Technol. Biotech.*, vol. 94, no. 8, pp. 2497-2511, 2019.
- [10] A. Kuvarega, N. Khumalo, D. Dlamini and B. B. Mamba, "Polysulfone/N,Pd co-doped TiO₂ composite membranes for photocatalytic dye degradation". *Sep. Purif. Tech*, vol. 19, no.1, pp. 122–133, 2018.
- [11] S. Hosseini, A. Prizeman, M. Aaron and A. E. Pirbazari, "Photocatalytic degradation of 2, 4-dichlorophenol by Co-doped TiO₂ (Co/TiO₂) nanoparticles and Co/TiO₂ containing mixed matrix membranes". *J. Water Process Eng.*, vol. 17, no. 10, pp. 124–134, 2017.
- [12] S. Teixeira, H. Mora, L. Blesse, P. M. Martins, S. A. C. Carabineer, S. Lanceros-Méndez, S. K. Kuhn and Cuniberti, "Photocatalytic degradation of recalcitrant micro pollutants by reusable Fe₃O₄/SiO₂/TiO₂ particles". *J. of Photochem. Photobio. A Chem.*, vol. 34, no. 5, pp. 27–35, 2017.
- [13] G. Boopathy, A. Gangasalam and A. Mahalingam, "Photocatalytic removal of organic pollutants and self-cleaning performance of PES membrane incorporated sulfonated graphene oxide/ZnO nanocomposite". *J. Chem. Technol. Biotech.*, vol. 91, no. 10, pp. 6462, 2020.
- [14] G. Shukla, K. Mishra and A. Khare, "Effect of the deposition, geometry on the electrical properties within Tin-doped indium oxide film deposited under a given RF magnetron sputtering condition". *J. of Alloys Compound*, vol. 489, no. 1, pp. 246–25, 2010.
- [15] P. Heinz-Helmut. "UV-VIS Atlas of Organic Compounds". 2nd ed., VCH, 1992.
- [16] K. Srivastava, M. Deepa, S. Bhandari and H. Fuess, "Method for the determination of the optical Dispersion characterization of sprayed Nickel mod". *Nanoscale Res. Lett.*, vol. 4, no. 1, pp. 54–62, 2009.
- [17] I. Hotovy, A. Pullmannova, M. Predanocny, J. Hotovy, V. Rehacek, T. Kups and L. Spiess, "Study of structural and optical properties of ZnS Nano structural thin films". *J. of Elect. Eng.*, vol. 60, no. 6, pp. 354–357, 2009.
- [18] W. Brown and W. W. Grannemann, "Anatase TiO₂ nanocomposite for Antimicrobial coating". *Solid State Electron*, vol. 21, pp.837–846, 1978.
- [19] J. Fidelus, M. Barczak, K. Michalak, Z. Fekner, A. Duzynska, A. Jusza, R. Piramidowicz, C. J. Monty and A. Suchocki, "Deposition of silver nanocomposite particles on titanium surface for antibacterial effect". *J. of Nanosci. Nanotech*, vol. 12, no. 1, pp. 3760–3765, 2012.
- [20] H. Liu T, C. Levy, and Z. Zhu, "Direct bandgap narrowing of TiO₂/MoO₃ hetero structure composites for enhanced solar-driven photocatalytic activity".

- Sol. Energy Mater. Sol. Cells, vol. 153, no.1. pp. 1–8, 2016.
- [21] D. Friedmann C. Mendive and D. Bahnemann, “TiO₂ for water treatment: Parameters affecting the kinetics and mechanisms of photocatalysis”. *Appl. Catal. B Environ.*, vol. 99, no. 4, pp. 398–406, 2010.
- [22] M. Alarm, A. Tewfik and S. Okawara, “Enhancement of photocatalytic activity of TiO₂ by immobilization on activated carbon for degradation of pharmaceuticals”. *J. Env. Chem. Eng.*, vol. 4, no. 2, pp. 1929–1937, 2016.
- [23] M. Eskandarian, M. Fazli, M. H. Rasoulifard and H. Choi, “Decomposition of organic chemicals by zeolite-TiO₂ nanocomposite supported onto low density polyethylene film under UV-LED powered by solar radiation. *Appl. Catal. B Environ.*, vol. 183, no. 1, pp.407–416. 2016.
- [24] J. Matos, J. Laine and J. M. Herrmann, “Effect of the type of activated carbons on the photocatalytic degradation of aqueous organic pollutants by UV-irradiated titania”. *J. of Catal.*, vol. 20, no.1. pp. 10–20, 2001.
- [25] A. Pal, T. K. Jana, and K. Chatterjee, “Silica supported TiO₂ nanostructures for highly efficient photocatalytic application under visible light irradiation”. *Mater. Res. Bull.*, vol. 76, no. 2, pp. 353–357, 2016.
- [26] M. Cui, S. Pan, Z. Tang, X. Chena, X. Qiao and Q. Xu, “Physiochemical properties of n-n heterostructured TiO₂/Mo-TiO₂ composites and their photocatalytic degradation of gaseous toluene”. *Chem. Speciat. Bioavailab.*, vol. 29, no. 1. pp. 60–69, 2017.
- [27] M. Buchi, P. Suresh, V. Biswas, R. Mahender and H. Johnson, “Comparative evaluation of electrical conductivity of hydroxyapatite ceramics densified through ramp and hold, spark plasma and post sinter Hot Isostatic Pressing routes”. *Mat. Sci. Eng. C*, vol. 70, no. 1, pp. 364–370, 2017.
- [28] P. Gifting, R. Bowen Dent I. Turner, F. R. Baxter and J. B. Chaudhuri, “Electrical characterization of hydroxyapatite-based bioceramics. *Acta Biomater.*, vol. 5, no. 2, pp. 743–754, 2009.
- [29] H. Nishikawa, “Surface changes and radical formation on hydroxyapatite by UV irradiation for inducing photocatalytic activation”, *J. of Mol. Catal. A Chem.*, vol. 20. No. 6. pp. 331–338, 2003.
- [30] Y. Chai, J. Ding, L. Wang, Q. Liu, J. Ren and W. L. Dai, “Enormous enhancement in photocatalytic performance of Ag₃PO₄/HAp composite: A Z-scheme mechanism insight”. *Appl. Catal. B Environ.*, vol. 179, no. 1, pp. 29–36, 2015.
- [31] A. Nevarez-Rascóna, A. Hurtado-Macías, H. Esperanza, M. Esparza-Ponce, M. Nevarez-Rascóna, J. González-Hernándezc, and M. J. Yacamán, “Nano-structured hydroxyapatite and titanium dioxide enriching PENTA /UDMA adhesive as aesthetic coating for tooth enamel”. *Acad. J. of Dental Mat.*, vol. 19, no. 1, pp. 37, 2021.
- [32] J. A. Nathanael, D. Mangalaraj and N. Ponpandian, “Controlled growth and investigations on the morphology and mechanical properties of hydroxyapatite/titania nanocomposite thin J. of films”. *Compos Sci. Tech.* vol. 70, no. 11, pp. 1645–1651, 2010.
- [33] M. Enayati-Jazi, M. Solati-Hashjin, M. A. Nemati and F. Bakhshi, “Synthesis and characterization of hydroxyapatite/titania nanocomposites using in situ precipitation technique. *Super lattices Microstruct.*, vol. 51, no. 2, pp. 85–877, 2012.
- [34] D. Z. Souri and I. Tahan, “A new method for the determination of optical band gap and the nature of optical transitions in semiconductor”. *J. of App. Sci.*, vol. 10, no. 6, pp.1103–1108, 2015.
- [35] K. Kaviyarasu, A. Mariappana, K. Neyvasagam, A. Ayeshamariam, P. Pandi, R. R. Palanichamy, C. Gopinathan, G. T. Mola and M. Maaza, “Photocatalytic performance and antimicrobial activities of HAp-TiO₂ nanocomposite thin films by sol-gel method”. *Surfaces & Interfaces*, vol. 6, pp. 247–255, 2017.
- [36] D. Hou, M. Zhuang, G. Zhang, M. Zhao and M.-S. Wu, “Solution processing of CuSe quantum dots: photocatalytic activity under RhB for UV and visible-light solar irradiation”. *J. of App. Surf. Sci.*, vol. 21, no. 8, pp. 97, 2003.
- [37] A. Balamurugan, G. Balossier, J. Michel and J.M.F. Ferreira, “Electrochemical and structural evaluation of functionally graded bioglass-apatite composites electrophoretic ally deposited onto Ti6 Al4 V alloy”. *Electrochimical Acta.*, vol. 54, no. 1, pp. 1192-1198, 2009.
- [38] K. Kaviyarasu, C. Maria Magdalane, E. Manikandan, M. Jayachandran, R. Ladchumananandasivam, S. Neelamani and M. Maaza, “Well-aligned graphene oxide nanosheets decorated with zinc oxide Nanocrystals for high performance photocatalytic application”. *Int J of Nanosci.*, vol. 14, no. 3, 1555007, 2015.
- [39] M. Nishikawa, W. Yang and Y. Nosaka, “Grafting effects of Cu²⁺ on the photocatalytic activity of titanium-substituted hydroxyapatite”. *Journal of Molecular Catalysis A: Chemical*. Vol. 378, pp. 314–318, 2013.
- [40] M. Ardyanian, M. M. Bagheri-Mohagheghi and N Sedigh, “Determination of the optimal parameter for the fabrication of ZnO thin films prepared by spray pyrolysis method”. *Pramana - J. of Phy.*, vol. 78, no. 4, pp. 625- 634, 2012.
- [41] F. Yakuphanoglu and H. Ertaen, Frequency independent- dependent conductivity and dielectric properties of some ionomers. *International J. of polymer*. Vol. 54, no. 1, pp. 1498–1501, 2005.
- [42] M. Aramendia, J. Hidalgo-Carrillo J, Sebti, “A study on the potential application of natural phosphate in

- photocatalytic processes". *J of Colloid and Interface Sci.*, vol. 344, no. 2, pp. 475-481, 2010.
- [43] J. shin, K. Lee, and I. Koh." Hydroxyapatite coating titanium dioxide thin films prepared by radio frequency magnetron sputtering." *J of Nanoscience and Nanotechnology*. Vol 13, no 8, pp. 5807 – 5810.
- [44] T. Nonami, H. Hase and K. Funakoshi, "Apatite-coated titanium dioxide photocatalyst for air purification". *Catalysis Today. J. of material sci.* vol. 96, no.1, pp. 113-11, 2004.
- [45] P. Sahay, R. Nath and S. Tewari, "Optical properties of thermally evaporated CdS thin films. *Cryst. Res Tech.*, vol. 42, no.1, pp. 275–80, 2007.
- [46] B. Elidnssi, M. Addou, M. Regragui, A. Bougrine and A.Kachouane, "Structural, composition and optical properties of ZnS thin films prepared by spray pyrolysis". *J. of Bernede, Mat. Chem. phys.*, vol. 68, no. 2, pp. 175–179, 2001.
- [47] J. Singh, John W, and sons, "Optical Properties of Condensed Matter and Applications" *J. of Non cryst solid.* vol. 1, no, 1, pp. 1- 10, 2006.
- [48] V. Bilgin, S. Kose, F. Atay and I. Akyuz, "The effect of substrate temperature on the structural and some physical properties of ultrasonically sprayed CdS films". *J. of Mat. Phys. Chem.*, vol. 94, no. 10, pp. 103–101, 2005.
- [49] S. Chakradar, G. Sivaramaiah, R. Lakshmana, N. O. Gopal, An alternative procedure for determination of the optical band gap and thicknesses of amorphous carbon nitride thin films., *J. of appl, surface science.* vol. 41, no. 2, pp. 271–80, 2008.
- [50] A. Part, Ehsani, M. H. Zareimoghadama, H. Rezagholi, and P. Kameli, "Surface modification of ZnS films by applying an external magnetic field in vacuum chamber". *J. of Mat. Res., Exp.*, vol. 62, no. 2, pp. 761, 2017.
- [51] K. Kawasaki, S Ikeda, Y. Takahashi and Y. Kuboki, "Further study of hydroxyapatite high performance liquid technique to increase chromatographic efficiency". *Euro. J. of Biochem.*, vol. 155, no. 7, pp. 249, 1986
- [52] J. Melsheimer and D. Ziegler, "Band gap energy and Urbach tail studies of amorphous, partially crystalline and polycrystalline tin dioxide". *Thin Solid Films, J. of applied physics.* vol. 129, no. 2, pp. 35–7. 1985.
- [53] V. Bilgin, S. Kose, F. Atay and I. Akyuz, "The effect of substrate temperature on the structural and some physical properties of ultrasonically sprayed CdS films". *J. of Mat. Phys. Chem.*, vol. 94, no. 1, pp.103–1016, 2005.